J. Fluid Mech. (1985), *vol.* 154, *pp.* 377–397
Printed in Great Britain

Self-sustained radial oscillating flows between parallel disks

By S. MOCHIZUKI† AND WEN-JEI YANG
Department of Mechanical Engineering & Applied Mechanics, The University of Michigan, Ann Arbor, Michigan 48109

(Received 20 February 1982 and in revised form 5 December 1984)

The flow-visualization methods of dye injection, hydrogen-bubble generation and paraffin mist are employed to investigate radial flow between parallel circular disks with a steady influx. Three distinct flow patterns are observed in the range of Re between 1.5 and 50. (1) Steady flow without boundary-layer separation and re-attachment, for $Re < Re_c$. (2) A self-controlled flow oscillation which decays further downstream, in the range of $Re_c \leqslant Re < Re_t$. (3) A self-sustained flow fluctuation which develops into a laminar–turbulent transition with a reverse transition further downstream, when $Re \geqslant Re_t$. Re_c and Re_t are the critical and transition Reynolds number, respectively.

The oscillating flows are caused by a vortex street consisting of vortices (i.e. separating annular bubbles) that separate periodically and alternately from both disks. Finite-difference solutions of the unsteady vorticity transport equation broadly agree with certain experimental observations. The study concludes that the separation and reattachment of shear layers in the radial flow through parallel disks are unsteady phenomena and the sequence of nucleation, growth, migration and decay of the vortices is self-sustained.

1. Introduction

Radial flow between parallel circular disks is of interest in a number of physical systems such as hydrostatic air bearings, radial diffusers and VTOL aircrafts with centrally located, downward-positioned jets. There exist two limiting cases in this flow: one is a creeping flow which occurs when the disk gap and flow rate are very small, i.e. the local Reynolds number is everywhere less than unity (Licht & Fuller 1954). This situation leads to a logarithmic decrease in the fluid pressure in the radial direction as the inertia effects become negligible in comparison to the viscous terms. The other extreme case is an incompressible, non-viscous flow in which the disk spacing and flow rate are large, i.e. the local Reynolds number is everywhere much greater than unity. Since the viscous effects become negligible, the Bernoulli equation yields a radially increasing pressure (Woolard 1954).

In most practical applications, the local Reynolds number lies between the above-mentioned extremes. Benenson & Bott (1961) obtained a solution for the radial pressure distribution using a Pohlausen method. The Kármán momentum-integral method was employed by Livesey (1960) for a more accurate solution, which was compared to experiments by Morgan & Saunders (1960). Sternberg (1954) dealt with the problem of a reverse transition from turbulent to laminar flow in the channel.

† On leave from Department of Mechanical Engineering, Tokyo University of Agriculture and Technology, Koganei, Tokyo, Japan.

Hunt & Torbe (1962) solved the Navier–Stokes equations for the velocity distribution in the flow by means of a power-series approach. The analysis was extended by Jackson & Symmons (1965*a*, *b*) to determine the pressure distribution. This solution is identical with that of Savage (1964), which was produced by perturbing the creeping-flow solution in terms of the downstream coordinate.

Moller (1963) carried out an extensive theoretical and experimental study of the problem. The results for both laminar and turbulent flows, obtained using an integral momentum method, agree well with experimental data. He concluded that (i) the critical Reynolds number (based on the mean velocity and the hydraulic diameter) is 2000 for reverse transition from turbulent to laminar flow; and (ii) the location of reattachment of the inlet-corner separation and the minimum-separation bubble pressure are functions only of the channel width at high flow rates. Jackson & Symmons (1965) performed experiments using two parallel disks with a very small central jet of 4 mm diameter and very small disk gaps (0.25, 0.5, 0.75, and 1.0 mm). It was concluded that the inertia effects predicted by the various theoretical analyses are significantly smaller than indicated by the experimental results.

Ishizawa (1965, 1966) combined a series-expansion method for the entrance region with a momentum-integral method for the downstream region. He predicted no separation below $Re = 100$ and double vortices at $Re = 200$. These conclusions were not confirmed by finite-difference solutions of the steady-state vorticity transport equation (Raal 1978). Wilson (1972) investigated the effects of different entry conditions. Raal concluded that, above $Re = 60$, separation is observed with the bubble size increasing rapidly with Re. He speculated on the existence of flow instability based on the observed concavity in the velocity profile for all $Re \geqslant 75$. Since Ishizawa (1965, 1966) and Raal (1972) dealt with the steady vorticity transport equation, their analyses cannot be applied to flow situations involving the formation of vortices.

The present work is concerned with the problem of instability in radial flow between parallel disks. Both the time-dependent numerical study and the experiments reveal the nucleation, growth, migration and decay of annular separation bubbles (i.e. vortex or recirculation zones) in the laminar-flow region. A finite-difference technique is employed to solve the full unsteady vorticity transport equation in the theoretical approach, while dye-injection, hydrogen-bubble and paraffin-mist methods are used to visualize the flow patterns. The experimental study also includes hot-wire measurements of the flow field. Theoretical predictions of the periodic and alternate formation as well as separation of vortices in the radial outward flow are confirmed by experiments.

2. Experimental approach

The methods of flow visualization and hot-wire measurement were employed to demonstrate that (i) vortex formation in radial flow through two parallel circular disks is, contrary to common belief, not a steady-state phenomenon and (ii) vortices separate periodically and alternately from both disks.

2.1. *Flow-visualization methods*

Both liquid- and gas-flow systems were visualized.

2.1.1. *Liquid flow system*

An experimental setup to visualize the flow patterns between parallel disks is shown in figure 1. The upper and lower disks, with 192 mm inside diameter (d_1) and 800 mm

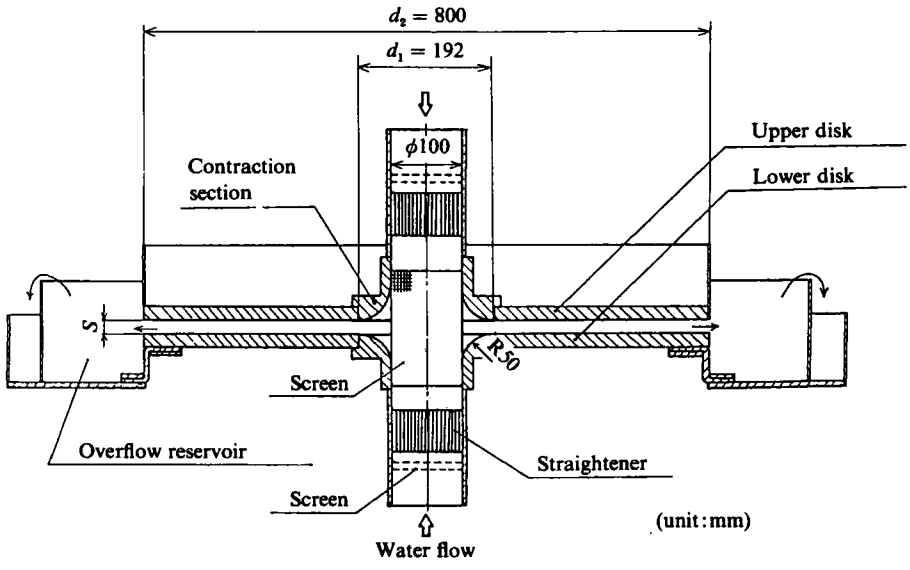

FIGURE 1. A schematic of the test apparatus.

outside diameter (d_2), were made of a 15 mm-thick transparent Plexiglas and a 20 mm-thick aluminium plate, respectively. The disk spacing (s) could be varied by adjusting six spacers installed at equal circumferential distance on the circumference of 780 mm diameter. Essentially no change in flow behaviour was detected when the number of spacers was varied between three and eight, or when the spacers were installed at different intervals on the same circumference. In order to produce a radial source flow, water from a constant-head overflow tank was divided into two streams, symmetrical but opposite in direction. After flowing through a symmetrical pair of screens and straighteners, the two streams were joined at the disk centre and flowed radially outward through a cylindrical screen mesh and a circular contraction section into the space between the parallel disks. The water was then collected in a circular overflow reservoir at the exit from the parallel disks. The flow rate of each of the two counter-flow streams was measured separately by a rotameter installed immediately downstream of the overflow tank. Both streams were adjusted to the same flow rate. The apparatus was firmly fixed on a support frame so that axisymmetry and uniform spacing between the disks could be maintained throughout an experiment.

The disk spacing was varied to give $s/d_1 = 0.026$, 0.052 and 0.078. The Reynolds number Re in the present study is defined as $(u_1 r_1/\nu)(s/d_1)^2$, where u_1 denotes the average inlet-flow velocity at r_1, the inner radius of the disks, and ν is the kinematic viscosity. The inlet-flow rate was varied to yield a range of Re from 7.9 to 50.

Ishizawa (1966) has presented a detailed argument on the definition of the Reynolds number for radial flow through parallel disks. When s/d_1 is sufficiently small, as in the present study, it does not explicitly affect the flow characteristics. Re is, therefore, defined as a product of $u_1 r_1/\nu$ and $(s/d_1)^2$ in the present work. However, for parallel disks having sufficiently large outer diameters, the flow phenomena are influenced by the two independent dimensionless parameters $u_1 r_1/\nu$ and s/d_1. The flow patterns were made visible by dye injection and hydrogen-bubble generation.

Hydrogen-bubble method. Figure 2 illustrates the setup for visualizing the flow by

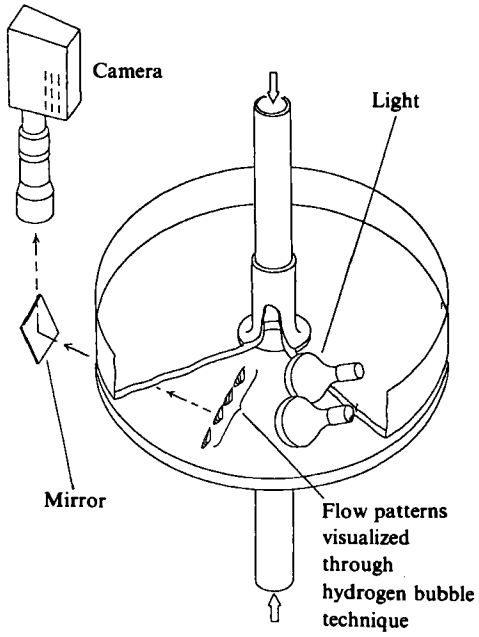

FIGURE 2. A schematic of the test setup for flow visualization by hydrogen-bubble generation.

the hydrogen-bubble method. Multiple fine platinum wires (50 μm in diameter) were installed perpendicularly between the disks at several radial locations along a radius. Hydrogen bubbles were generated from the wires through the application of pulsating electric current. Under illumination by photoflood lamps, the image was reflected by a mirror into a camera or a video camera. The video pictures were analysed for unsteady-flow phenomena using a slow–still motion analyser.

The effect of bubble-generating wires on the flow pattern is well documented in a number of references, for example Schraub *et al.* (1965) and Davis & Fox (1967) and hence is not repeated here. The presence of the wire is entirely irrelevant in the present application since its sole mission is to detect the occurrence of vortex formation rather than the quantitative determination of time-dependent velocity fields.

Some representative results are shown in figures 3(*a*) and (*b*) for s/d_1 of 0.078 and 0.026, respectively. The horizontal coordinate X is a dimensionless radial defined as $(r-r_1)/\frac{1}{2}s$. $X = 0$ corresponds to the entrance at r_1, while the exit is at $X = 40.6$ for $s/d_1 = 0.078$, or at $X = 121.8$ for $s/d_1 = 0.026$. Both figures show almost uniform velocity profiles at the entrance, irrespective of Re and s/d_1. For the lower Re flow corresponding to case *a* in both figures, the velocity profile gradually develops into a fully developed parabolic shape. As Re is increased to, or beyond, a critical value Re_c, flow separation occurs alternately from both walls at the same radial location X_s, as indicated by an arrow. Downstream from the separation point, the free shear layer becomes curled up and stretched for a considerable distance. The double vortices generated periodically and alternately on both walls form a vortex street, as seen in case *b* of figure 3(*a*) and cases *c*, *d* of figure 3(*b*). As Re is increased further to or beyond Re_t, as in case *c* of figure 3(*a*) and case *d* of figure 3(*b*), the flow oscillations due to the vortex streets develop into turbulent flow. However, when the velocity, which decreases with increasing radius, has been reduced sufficiently, a reverse

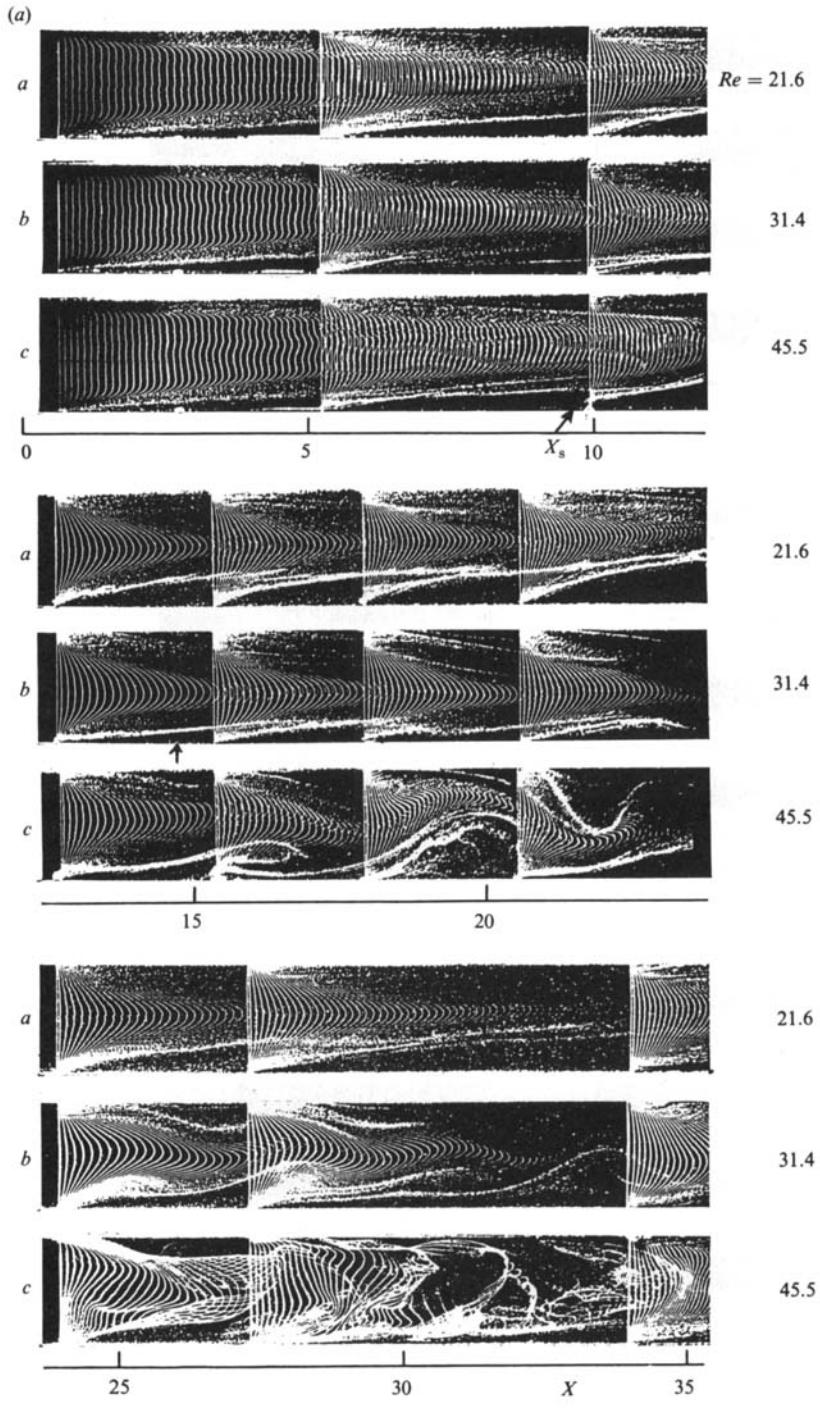

Figure 3(*a*) For caption see next page.

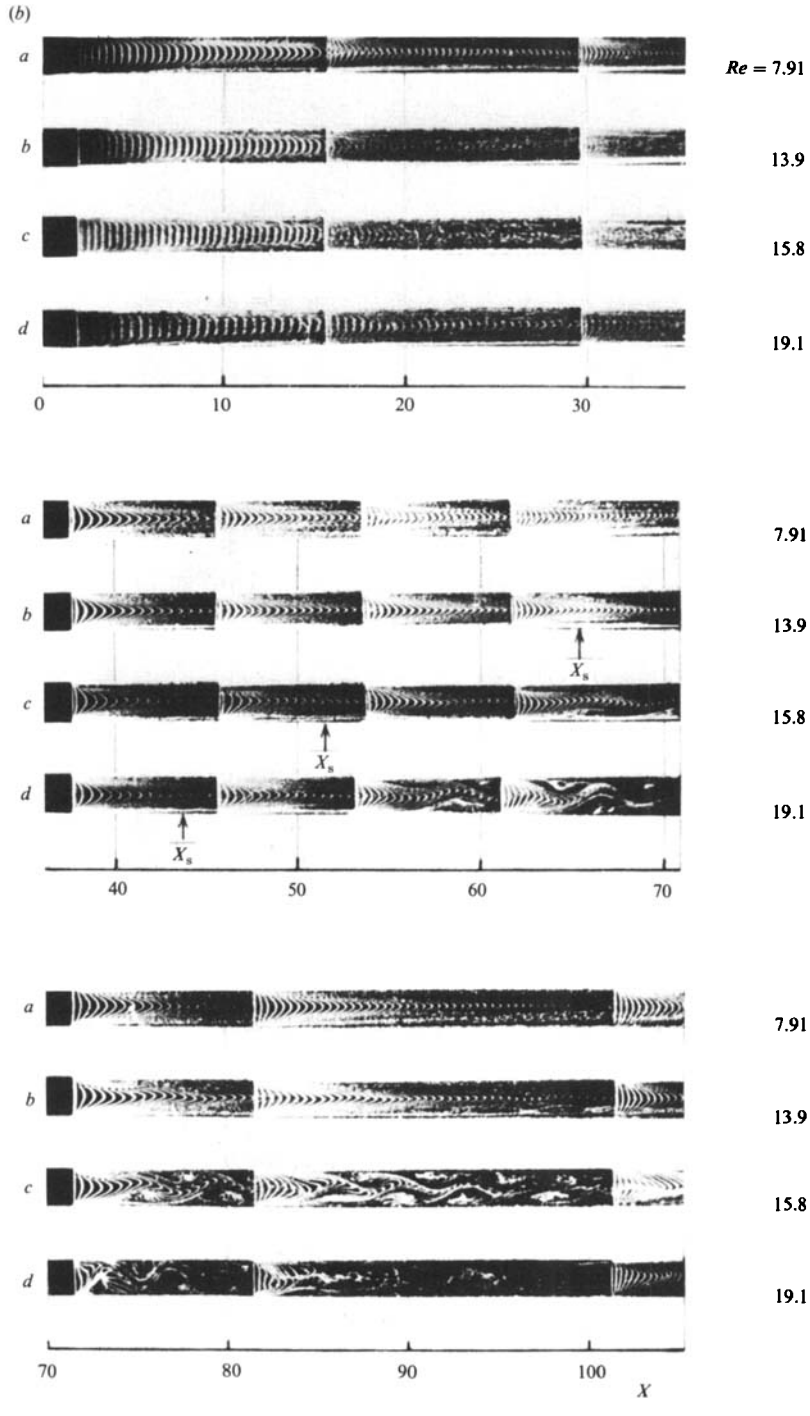

FIGURE 3. Photographs of flow patterns between parallel disks: (*a*) $s/d_1 = 0.078$ at $Re = 21.6$, 31.4 and 45.5; (*b*) $s/d_1 = 0.026$ at $Re = 7.91$, 13.9, 15.8 and 19.1.

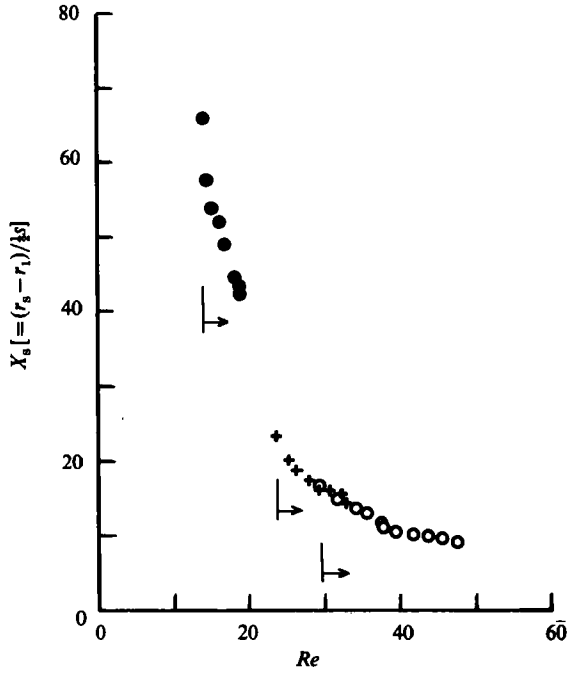

FIGURE 4. Test results for separation point r_s as a function of Re for $s/d = 0.078$, (○○○), 0.052 (+ + +) and 0.026 (●●●).

transition from turbulent to laminar flow takes place. It is important to note that these still photographs have revealed the occurrence of unsteady separation phenomena, but are not suitable for demonstrating annular separation bubbles. An examination of the video movie films playing at a low speed or frame by frame did show the formation of annular separation bubbles. The locations of X_s in figures 3 (*a*) and (*b*) were thus determined. The separation point moved upstream with an increase in Re. Figure 4 is a plot of X_s versus Re_t obtained from the visualization study. The radial location of the separation point is r_s. The vertical line with a horizontal arrow designates the critical Reynolds number Re_c for separation to occur. This correlation leads to the conclusions that (i) Re_c increases with s/d_1, (ii) irrespective of s/d_1, the location of the separation point is determined only by Re, and (iii) the separation point moves upstream as Re is increased.

Dye-injection method. A white poster-colour dye was injected into the radially outflowing stream at the centre $r = 0$ between the two parallel disks. Observations and photographic recordings were made directly through the transparent upper disk with illumination by photoflood lamps. At a certain radial location, a ring of near-circular white roll cells was observed to form spontaneously which then propagated downstream (in other words, the ring diameter expanded radially outward). The cells were produced by the concentration of the dye resulting from vortex formation. The phenomenon could be clearly observed by the naked eye. However, if the camera was positioned to cover the entire disk surface, then the flow pattern appeared blurred in the photo, so only part of the roll-cell ring was photographed, as shown in figure 5. It covers the flow area confined between the two radial lines in the left figure, as viewed from above. The photograph covers the rectangular area shown in the figure. For s/d_1 of 0.026, figure 4 indicates that vortex

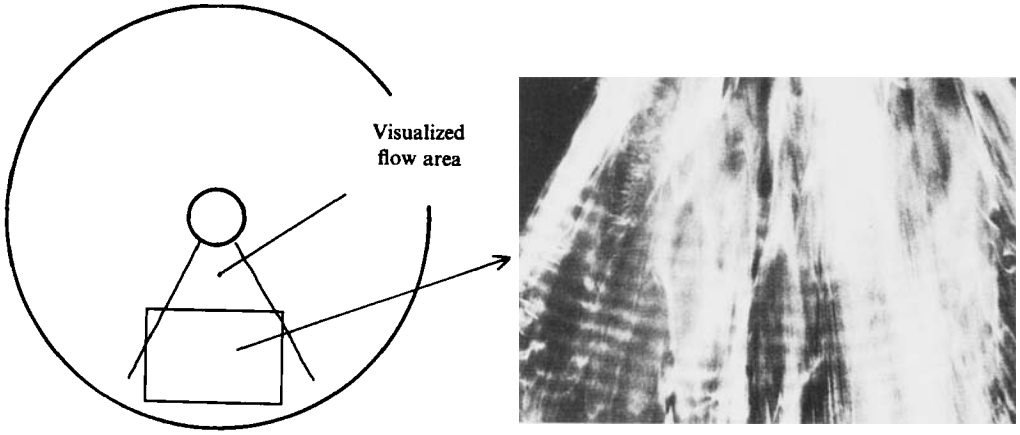

FIGURE 5. Photographs of flow patterns in parallel disks with $s/d_1 = 0.026$ at $Re = 14.5$, visualized by dye injection.

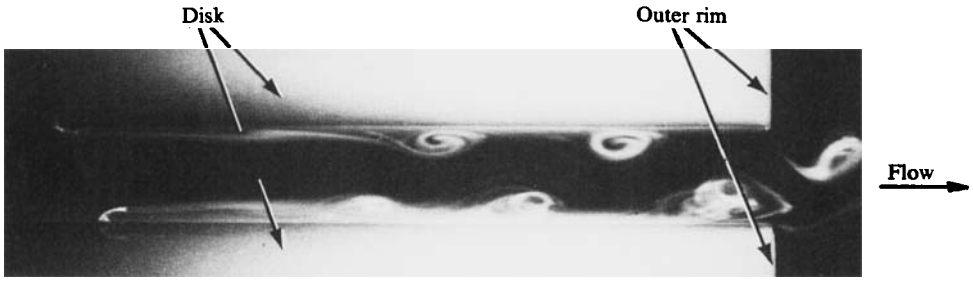

FIGURE 6. Vortex formation in the radial flow through two parallel circular disks visualized by the paraffin-mist method.

separation occurred at a value of Re_c between 13 and 14. Since the photo corresponds to $s/d_1 = 0.026$ and $Re = 14.5$, vortex formation should have occurred. They indeed appeared as bands of circular arc, indicating an axisymmetrical nature of vortex formation.

2.1.2. *Gas-flow system by paraffin-mist method*

Even in a pair of parallel disks without a spacer, our separate study produced figure 6, revealing the occurrence of periodic vortex formation. The photo illustrates the visualization of the air stream by means of paraffin mists. Hence the periodic vortex formation is a phenomenon of unusually strong character which is unaffected by the presence of spacers or hydrogen-generating wires.

2.2. *Hot-wire measurements*

In contrast to the use of water in the flow-visualization test, the velocity variations of air in the radial flow between two parallel circular disks were measured by hot wires at various radial locations. Figure 7 depicts a schematic diagram of the test apparatus. The output of the hot wires was fed into a Hewlett Packard Type 3582A, 2-channel real spectrum analyser. Results from the analyser were recorded on an X–Y plotter. Figure 8 shows the locations at which hot-wire measurements were made. Eleven 10 mm-diameter holes were drilled on an acrylic disk between $r = 135$ and

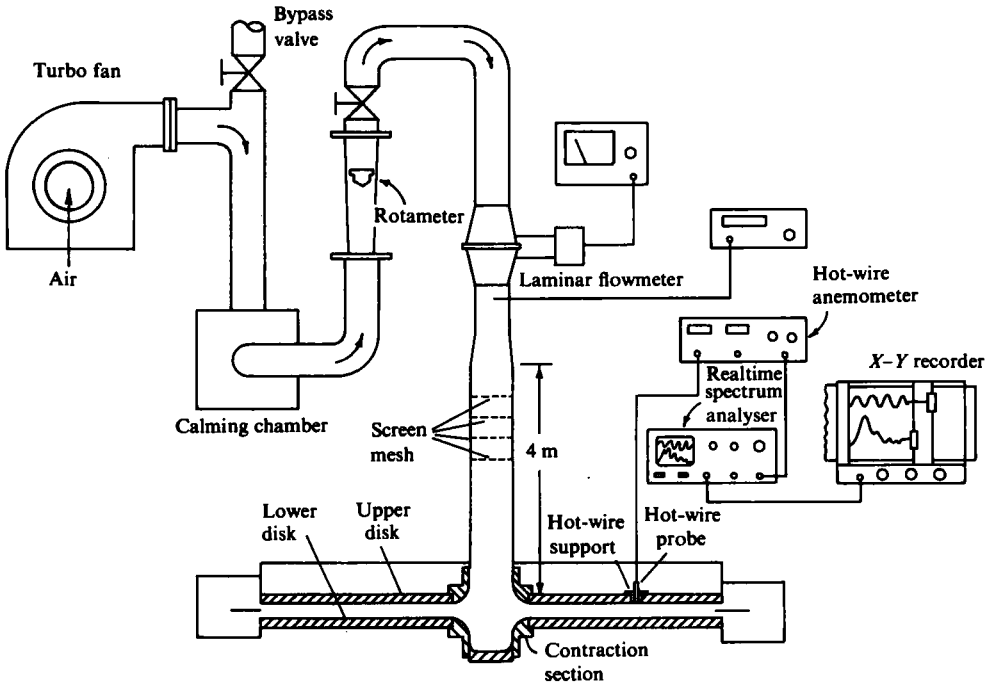

FIGURE 7. A schematic of the test apparatus for hot-wire measurements.

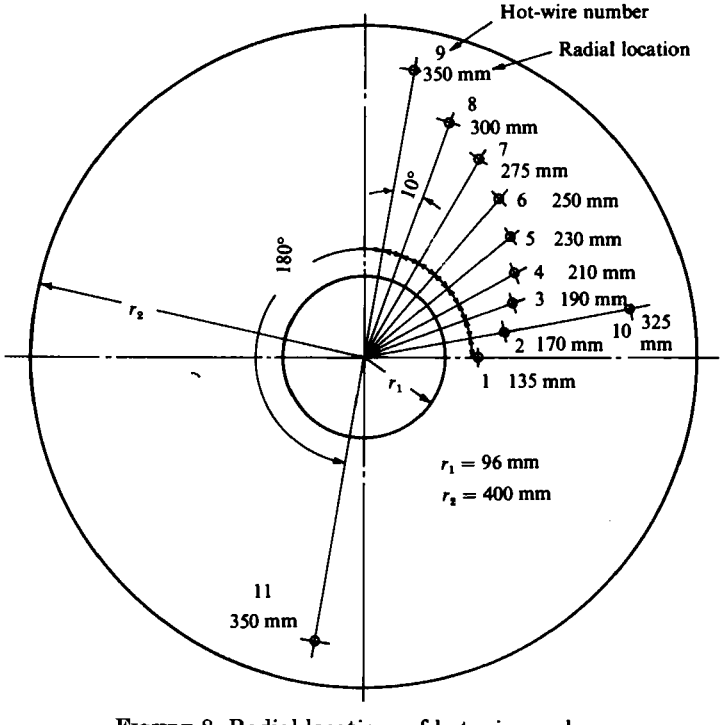

FIGURE 8. Radial locations of hot-wire probes.

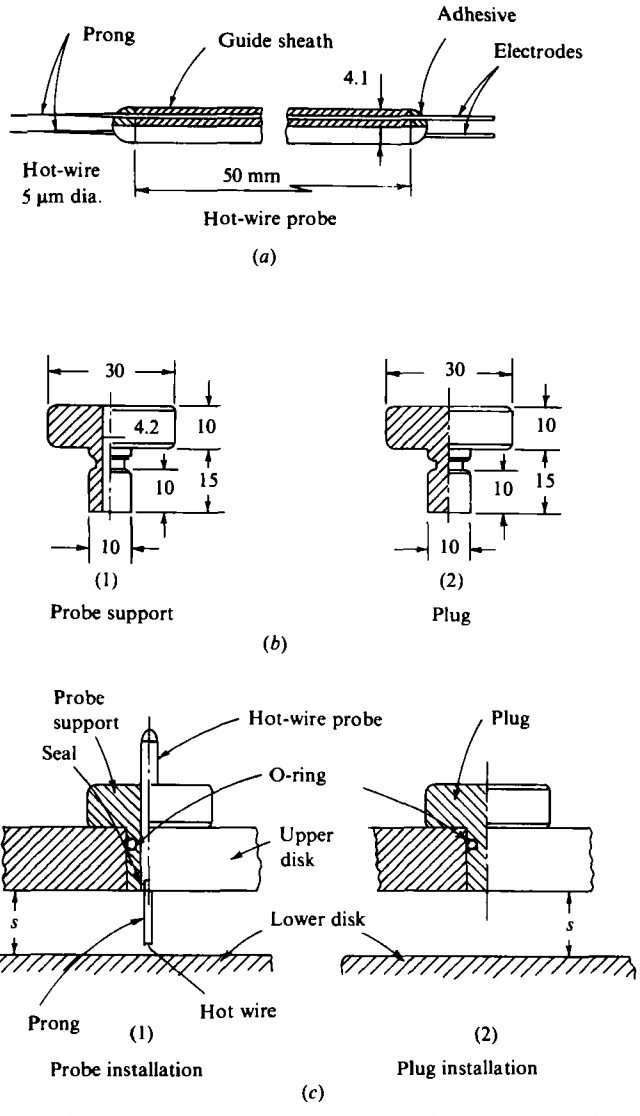

FIGURE 9. Details of (*a*) hot wire, (*b*) plug and (*c*) their installations.

350 mm. Each hole was fitted with a hot-wire probe or a plug when flow measurement was not needed. The details of a hot-wire probe, its support, a plug and their installations are depicted in figure 9. Figure 10 shows the recording of radial-velocity variations monitored by two hot wires which were positioned at mutually symmetrical positions, nos. 9 and 11 as shown in figure 8. It is seen that the waveforms of the two radial velocities were very similar and of the same frequency. This observation confirms the axisymmetry of vortex-generation phenomena. The phase shift between the two waves was probably due to a slight deviation of the radial velocities in the circumferential direction.

From the two experiments described in §§ 2.1 and 2.2, it is concluded that vortex formation is axisymmetrical in nature.

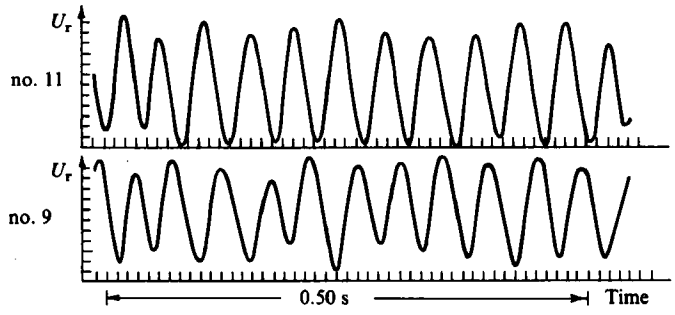

FIGURE 10. Variation of radial velocities at location nos. 9 and 11 in parallel disks with $s/d_1 = 0.052$ and $Re \cong 25$.

3. Theoretical approach

3.1. *Formulation of the problem*

The physical system to be studied is shown in figure 11. It consists of two parallel disks with inner radius r_1. An incompressible fluid flows radially outward through the spacing s, between the disks. The origin of the cylindrical coordinates (r, θ, z) is fixed at the centre 0. With the use of the stream function ψ defined as:

$$U = \frac{1}{R}\frac{\partial \psi}{\partial Z}, \quad W = \frac{1}{R}\frac{\partial \psi}{\partial R}, \tag{1}$$

the unsteady vorticity transport equation for an axisymmetrical flow can be written as:

$$\frac{\partial \omega}{\partial \Theta} + \frac{1}{R}\frac{\partial \psi}{\partial Z}\frac{\partial \omega}{\partial R} - \frac{1}{R}\frac{\partial \psi}{\partial R}\frac{\partial \omega}{\partial Z} - \frac{1}{R}\frac{\partial \psi}{\partial Z}\omega = \frac{(s/d_1)^2}{Re}\left(\frac{\partial^2 \omega}{\partial R^2} + \frac{1}{R}\frac{\partial \omega}{\partial R} - \frac{1}{R^2} + \frac{\partial^2 \omega}{\partial Z^2}\right), \tag{2}$$

wherein the vorticity is

$$\omega = \frac{1}{R}\left(\frac{\partial^2 \psi}{\partial Z^2} + \frac{\partial^2 \psi}{\partial R^2} - \frac{1}{R}\frac{\partial \psi}{\partial R}\right). \tag{3}$$

Here, the variables are defined in dimensionless form as:

$$R = \frac{r}{r_1}, \quad Z = \frac{z}{r_1}, \quad U = \frac{u}{u_1}, \quad W = \frac{w}{u_1}, \quad \Theta = \frac{u_1 \tau}{r_1}, \tag{4}$$

where τ is the time. By means of the transformation

$$Y = 1 - \frac{1}{R}, \tag{5}$$

(2) and (3) become respectively

$$\frac{\partial \omega}{\partial \Theta} + (1-Y)^3\frac{\partial \psi}{\partial Z}\frac{\partial \omega}{\partial Y} - (1-Y)^3\frac{\partial \psi}{\partial Y}\frac{\partial \omega}{\partial Z} - (1-Y)^2\frac{\partial \psi}{\partial Z}\omega = \frac{1}{Re}\left\{(1-Y)^4\frac{\partial^2 \omega}{\partial Y^2} - (1-Y)^3\frac{\partial \omega}{\partial Y} - (1-Y)^2 + \frac{\partial^2 \omega}{\partial Z^2}\right\}, \tag{6}$$

and

$$\omega = (1-Y)\left\{\frac{\partial^2 \psi}{\partial Z^2} + (1-Y)^4\frac{\partial^2 \psi}{\partial Y^2} - 3(1-Y)^3\frac{\partial \psi}{\partial Y}\right\}. \tag{7}$$

Equations (6) and (7) are subject to the following boundary conditions:

Uniform flow with zero vorticity is imposed at the disk entrance, yielding

$$\psi = Z, \quad \omega = 0 \quad \text{at } Y = 0. \tag{8}$$

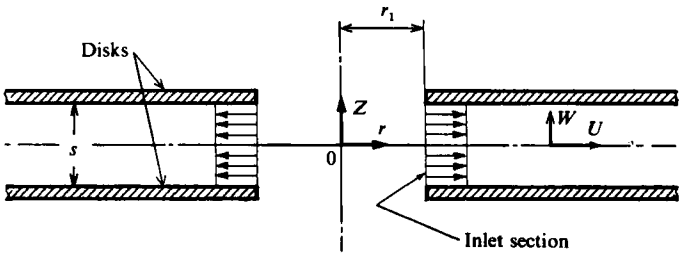

FIGURE 11. Parallel disks and coordinates.

The flow profile acquires a fully developed parabolic shape at large distances downstream, Y_∞, which gives

$$\psi = \frac{1}{2}\left\{3Z - \left(\frac{d_1}{s}\right)^2 Z^3\right\}, \quad \omega = -3(1-Y)\left(\frac{d_1}{s}\right)^2 Z \quad \text{at } Y = Y_\infty. \tag{9}$$

The no-slip condition along the disk surfaces yields:

$$\psi = \pm\frac{s}{d_1}, \quad \omega = (1-Y)\frac{\partial^2\psi}{\partial Z^2} \quad \text{at } Z = \pm\frac{s}{d_1}. \tag{10}$$

3.2. *Solution procedure*

The governing equation (6) and the associated expression for vorticity (7) were reduced to a set of simultaneous, algebraic finite-difference equations, which related the values of the variables at each nodal point to the values at neighbouring grid points. This set of algebraic equations together with suitable boundary conditions was then solved on a digital computer.

The following computational procedure was employed: (i) Initially, the entire flow field for $Re = 32.4$ was set at a fully developed laminar pattern under a no-slip condition between two parallel disks. Since asymmetry in the boundary conditions was necessary to create a disturbance in the flow field, a slip condition (any values of ψ and ω, for example $\psi = s/d_1$ and $\omega = 1$) was suddenly imposed on one section of the upper (or lower) disk wall (for example, $Y = 0.18$ to 0.38). After a brief period of the computing operation (Θ ranging from 0 to 0.25), the slip condition was switched to a non-slip one. In all other Re cases, the numerical procedure was initiated using the flow field for $Re = 32.5$ at $\Theta = 96.0$ as an initial value at each nodal point. (ii) An alternating-direction implicit method was employed to solve the finite-difference expressions of (6) for the new values of ω at interior grid points. On the other hand, the new values of ψ were determined from the finite-difference form of (7) by applying a successive over-relaxation technique to it in finite-difference form, swept through the computational grid line by line in the interior points. A relaxation factor of 1.82 was employed to accelerate convergence of the iteration process. (iii) Solutions were considered to have converged when the current value ψ^{n+1} deviated from its previous value ψ^n by less than 10^{-8} at all grid points. (iv) The values of ω on the wall were calculated using Jensen's (1959) formula:

$$\omega_w = \frac{(-7\psi_w + 8\psi_{w+1} - \psi_{w+2})(1-Y)}{2(\Delta Z)^2}, \tag{11}$$

where the subscripts w, w+1 and w+2 indicate the nodal points on the wall, and at one and two locations from the wall, respectively. (v) Step (ii) was repeated until

the values of ω and ψ at all interior points were evaluated. (vi) Computations were terminated whenever a steady-flow situation in the case of low-Re flow or a limit-cycle (self-sustained) condition in the case of high-Re flow resulted. (vii) Streamwise and transverse velocity components were determined from their respective definitions.

The flow field (Y, Z)-plane for $s/d_1 = 0.075$ was subdivided into a 50×40 uniformly spaced grid network (with 50 nodes in the radial direction and 40 nodes in the transverse direction). The corresponding mesh size was $\Delta Y = 0.02$ by $\Delta Z = 0.00375$. The time increment $\Delta\Theta = 0.0005$ was employed in numerical computations for $Re = 5.0$, 10.0, 20.0, 25.0, 27.5, 28.5, 29.0, 30.0, 32.5, 34.0, 35.0, 37.5, and 40.0 while $\Delta\Theta$ of 0.001 was used for $Re = 1.25$. Numerical experiments with $\Delta\Theta$ varying from 0.001 and 0.005 were performed to examine the convergence of the computer solutions for $Re = 20.0$, 30.0 and 37.5. The flow-field variations were practically identical for $\Delta\Theta$ of 0.002 and 0.005. In case of $Re = 1.25$, the computer solution converged for $\Delta\Theta$ equal to or less than 0.05.

The value of Y_∞ depended on the disk size since it is defined as $1 - r_2/r_1$. Numerical experiments were conducted for both $Re = 20$ and 30. In each Re, results were almost identical for three values of Y_∞ (1, 0.999 and 0.995, corresponding to $R = \infty$, 1000 and 200, respectively). The value of Y_∞ in the experimental study is 0.76.

Numerical integrations were performed using an HITAC M-200H System digital computer. The CPU time ranged from 6 to 208 minutes depending upon Re and the nature of each flow. When the Reynolds number exceeds a critical value Re_c this asymmetrical flow caused amplification of unstable disturbances, resulting in the formation of vortices. At a Reynolds number of 27.5 which is below the critical value, however, the asymmetry decayed rapidly and computation led to a steady-flow situation. At higher Reynolds numbers of 30.0, 32.5 and 34.0, self-sustained flow oscillations occurred. Therefore Re_c lies between 27.5 and 30.0.

When Re exceeded 35.0, numerical instabilities resulted in the divergence of the computations. Re_t denotes the Reynolds number for the onset of divergence in the computations of the flow field.

3.3. *Computations for various Reynolds numbers*

3.3.1. $Re < Re_c$

Figure 12 shows the timewise variation of the radial velocity U for $Re = 27.5$ at various locations a, b, c, d, e and f, identified in figure 13. The asymmetrical flow pattern introduced as the initial condition triggered flow pulsations which diminished with time. It is interesting to compare the transient behaviour of points c, d and e, which were at the same radial distance $X = 13.3$ but different transverse locations $Z = 0.045$, 0 and -0.045, respectively. The oscillation at point d on the plane of symmetry decayed very rapidly. The fluctuating patterns of points c and e are identical except for a phase difference of 180°. After a large time has elapsed, the entire flow field becomes steady with the velocity distribution being symmetrical with respect to the radial axis. Some representative velocity profiles at the final steady state are illustrated in figures 14, 15, and 16 for $Re = 1.25$, 10.0 and 20.0, respectively. In all cases, the uniform inlet profile has entrance-region distance. However, the smaller the Re, the shorter is the entrance region, due to a more rapid development of the boundary layer. Points of inflexion were visible in some velocity profiles for $Re = 20.0$. These occurred near the entrance, owing to the boundary-layer development. This phenomenon, usually associated with flow instability, was confirmed by the experimental results using flow visualization, as seen in figures 3 (a) and (b). This is a singular feature of radial flow which cannot be observed in pipe flows. The numerical

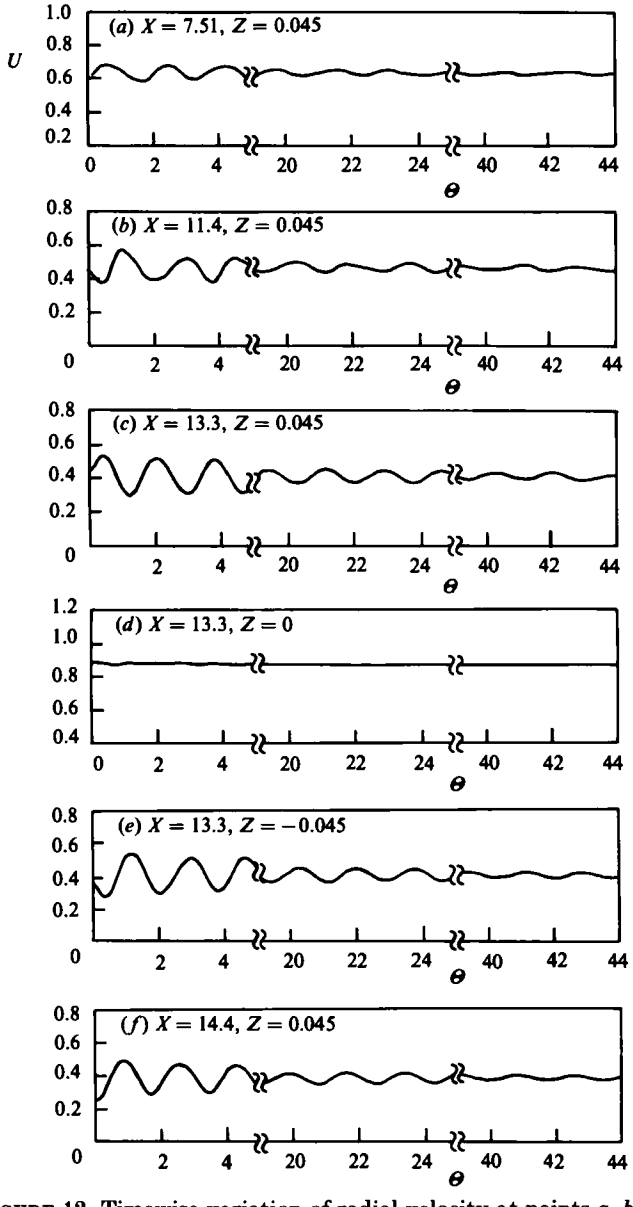

FIGURE 12. Timewise variation of radial velocity at points *a*, *b*, *c*, *d*, *e* and *f* in parallel disks with $s/d_1 = 0.075$ at $Re = 27.5$.

results for low-Re flow, not shown here, confirmed the observation that a strong adverse pressure gradient developed along the wall near the entrance (Ishizawa 1966; Raal 1978). The steady-state profiles, figures 14, 15 and 16, almost coincide with the theoretical results of Ishizawa (1965, 1966), obtained by the combined series-expansion–momentum-integral method.

3.3.2. $Re_t > Re \geqslant Re_c$

The flow field which began with an asymmetric pattern experienced a transient period during small times. The flow then reached a limit-cycle state in which a periodic generation of vortices occurred alternately from both disk walls. Figure 17

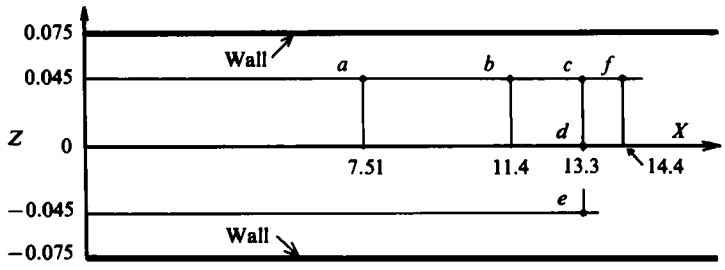

FIGURE 13. Location of points a, b, c, d, e and f in parallel disks.

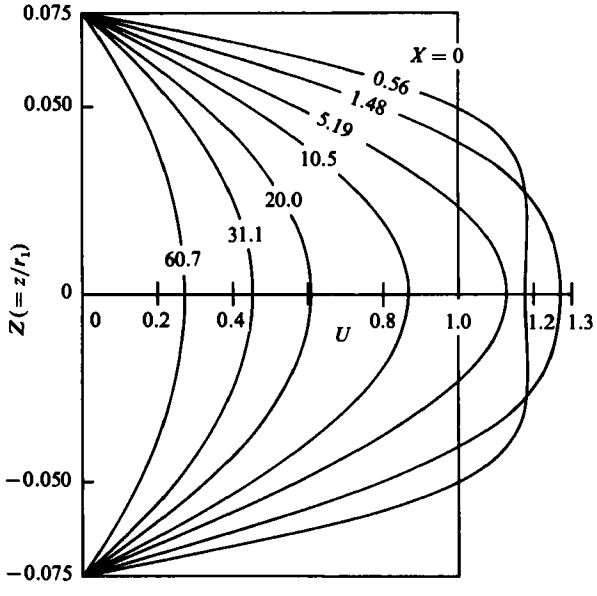

FIGURE 14. Profiles of radial velocity at various radial locations in parallel disks with $s/d_1 = 0.075$ at $Re = 1.25$.

illustrates the timewise variation of the radial velocity U for $Re = 34.0$ at various locations a, b, c, d, e and f. As will be disclosed later in figure 19, point a at $X = 7.51$ was a short distance upstream from the separation point. The flow oscillation there was not sinusoidal, as shown in figure 17 (a). However, as the flow passed downstream through points b, c, d, e and f, the shape of the flow pulsation approached a sinusoidal form. The non-dimensional period of oscillation decreased very slightly with increasing Re, i.e. 1.78, 1.76 and 1.75 for $Re = 30.0$, 32.5 and 34.0 respectively. As in the previous case of $Re = 27.5$, the flow oscillations at points c and e were nearly the same in shape and amplitude except for a phase difference of 180°. However, their frequency was one-half that of the flow pulsation at point d on the plane of symmetry between the disk walls. Figure 18 demonstrates the variation of the radial velocity profiles at $X = 13.3$ over approximately one cycle, i.e. between the instants 1 and 5, which correspond to $\Theta = 71.05$ and 72.80, respectively. The phase angle between two consecutive instants was approximately 90°. It is observed that the maximum-velocity and the reverse-flow region near the wall occurred alternately on both sides of the plane of symmetry ($Z = 0$). Although instants 1 and 5 correspond to the beginning and end of the cycle, respectively, their radial-velocity profiles were not perfectly

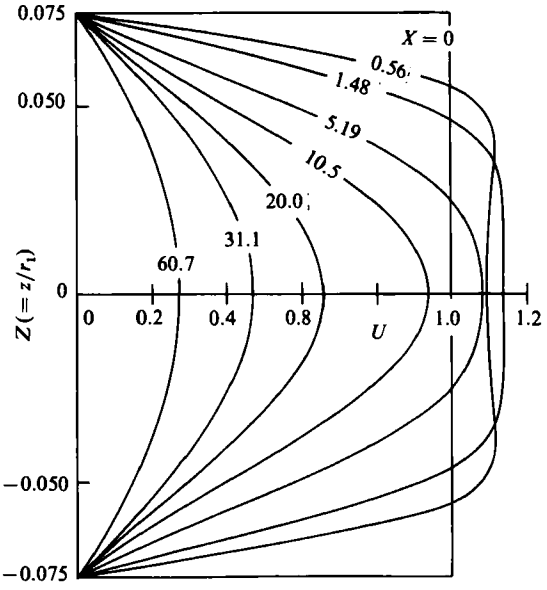

FIGURE 15. Profiles of radial velocity at various radial locations in parallel disks with $s/d_1 = 0.075$ at $Re = 10.0$.

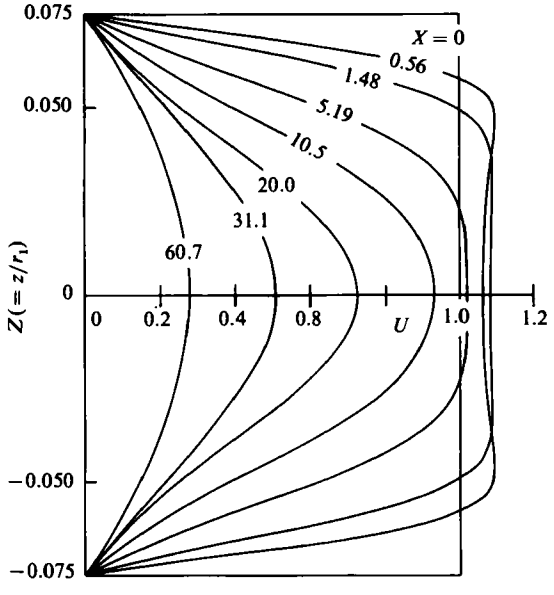

FIGURE 16. Profiles of radial velocity at various radial locations in parallel disks with $s/d_1 = 0.075$ at $Re = 20.0$.

identical because the oscillating-flow phenomena changed slightly from cycle to cycle. It was disclosed that an increase in Re promoted an enlargement of the reversed-flow region together with a shift in the location of the maximum velocity toward the disk walls. Figure 19 was obtained by plotting the streamlines at approximately 90° intervals over the entire cycle of the flow pulsation, i.e. $\Theta = 71.05$ to 72.80. Cases

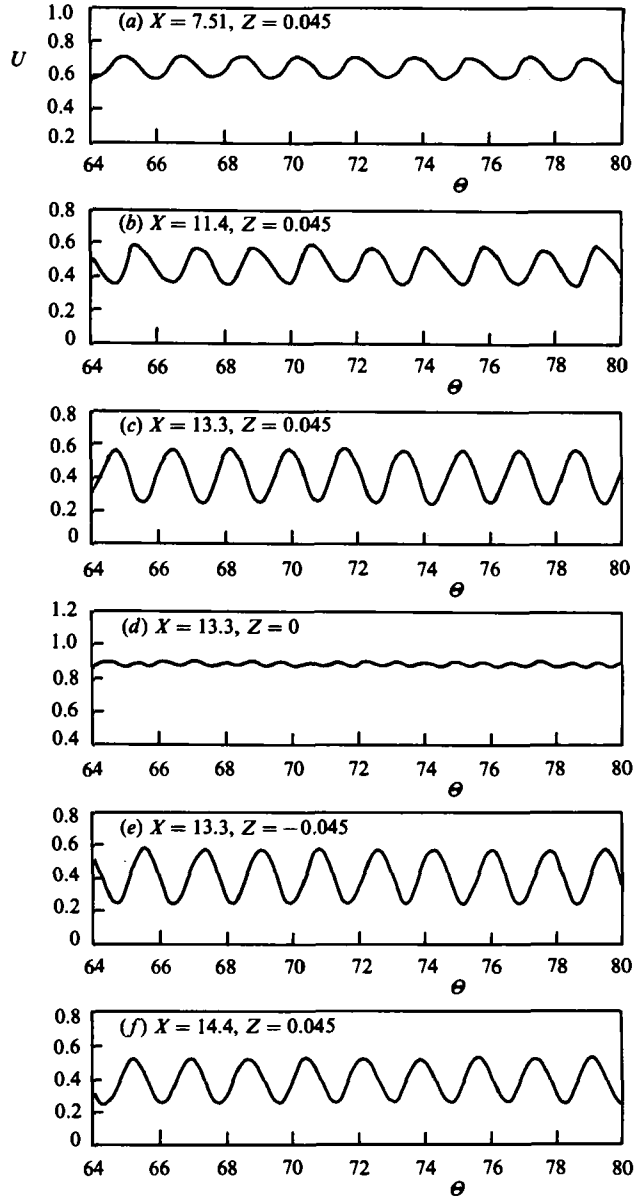

FIGURE 17. Timewise variation of radial velocity at points *a*, *b*, *c*, *d*, *e* and *f* in parallel disks with $s/d_1 = 0.075$ at $Re = 34.0$.

1–5 correspond to the time instants 1–5 in figure 18. First, one sees the nucleation of an annular separation bubble at X of approximately 8.5 on the upper disk. After growing to a certain size, as seen in case 1, the bubble migrated along the wall as is shown consecutively in cases 2–5. During the course of the excursion, its size diminished gradually. After a certain duration of time, the bubble resembled the second one on the upper disk in case 1. It continued to move downstream with diminishing size, as seen in cases 2 and 3, and finally disappeared from the wall, case 4. The disappearance triggered the formation of an embryo upstream at the same

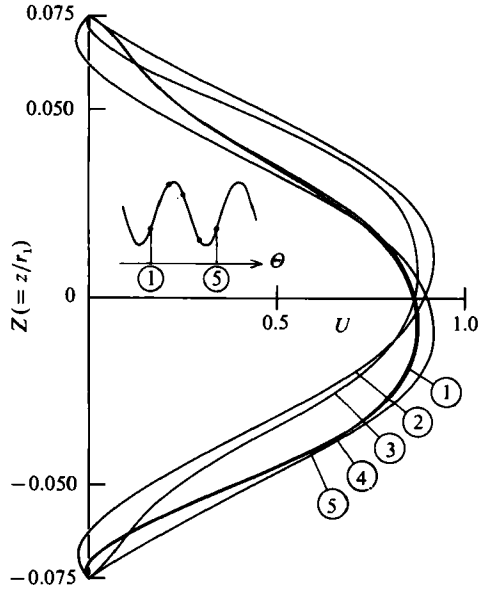

FIGURE 18. Timewise variation of radial velocity profile at $X = 13.3$ in parallel disks with $s/d_1 = 0.075$ at $Re = 34.0$.

nucleation site, which can be seen as the left bubble on the upper disk in case 4, which had already grown substantially. The cycle is self-sustaining. A bubble was alternately formed at the same radial distance on the lower-disk wall; the nucleation occurred sometime after the bubble on the upper wall departed from the nucleation site, the bubble undergoing the same cycle of nucleation, growth, migration and decay as its counterpart on the upper wall. Two bubbles were always on each disk, forming a vortex street. These vortices caused oscillations in the flow, which were rapidly damped out downstream from the site of disappearance. The flow then gradually redeveloped further downstream into a parabolic profile. The existence of fluctuations in radial flow between parallel disks has remained undetected because it decayed before reaching the plate exit, where flow measurements would register only steady-velocity profiles.

Although the results for other Reynolds-number flows are not included here, in the interest of brevity, the nucleation site was found to move upstream with an increase in *Re*.

Bakke, Kreider & Kreith (1973) performed an experimental study of the velocity and turbulence fields in the gap between two parallel co-rotating or stationary disks with a source in the centre. This was achieved by hot-wire measurements over a wide range of source strengths and disk speeds. In section VI-A entitled 'Radial Poiseuille flows', Narasimha & Sreenivasan (1979) reviewed the literature on relaminarization of flows through two parallel co-rotating or stationary disks. A plot of the critical Reynolds number versus the radius for the onset of relaminarization defined the transition/ reversion boundaries in radial Poiseuille flow. Both references treat a single stream with parabolic velocity profile at the entrance, while the present study is concerned with two counter-flow streams with uniform velocity profiles at the entrances. The difference in the entry conditions makes it meaningless to compare the results on relaminarization between the two cases.

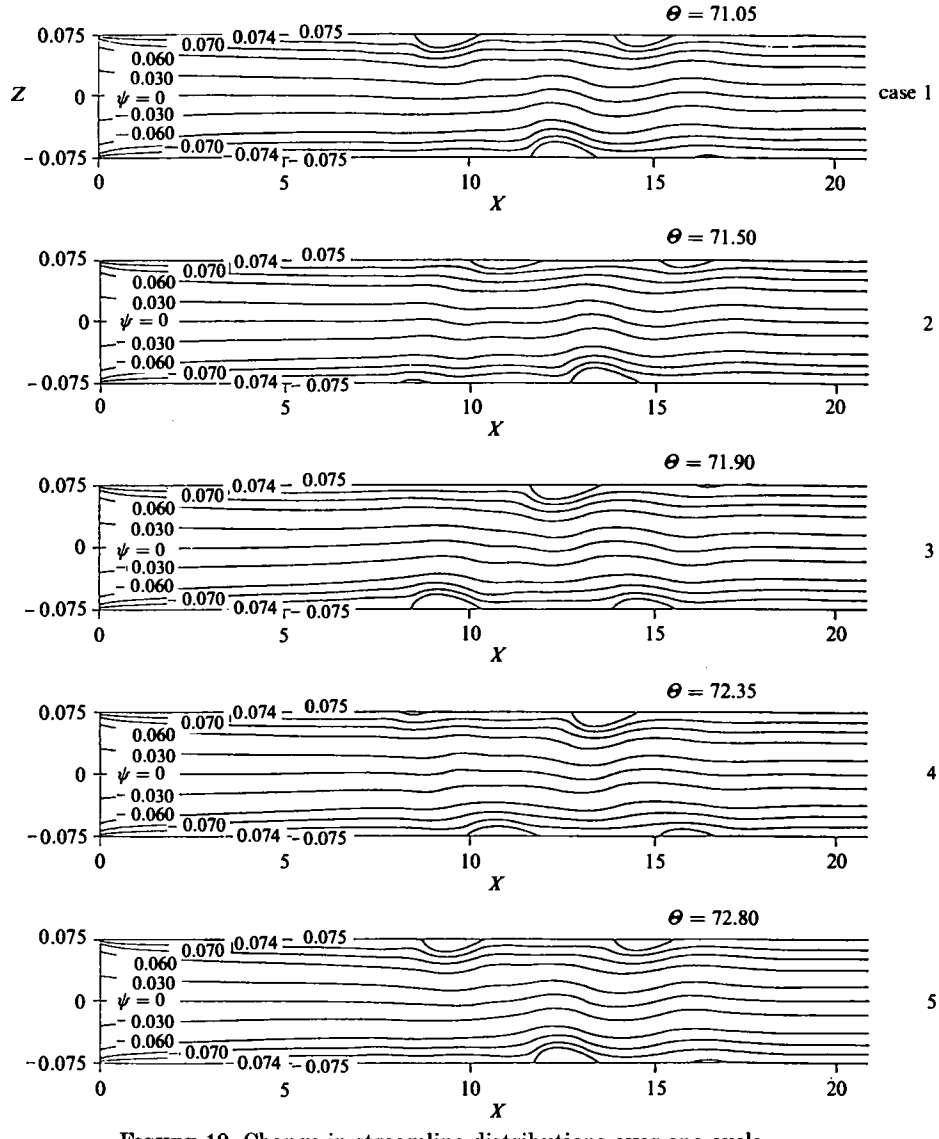

FIGURE 19. Change in streamline distributions over one cycle in parallel disks with $s/d_1 = 0.075$ at $Re = 34.0$.

3.3.3. $Re \geqslant Re_t$

When the Reynolds number Re exceeds a critical value Re_t (35.0 in the present study), the oscillations of the flow field initiated at small times from an asymmetrical initial flow distribution, are amplified gradually with time. Eventually, the numerics of computation result in a divergence of the computed results at a location downstream from the inlet corner. The termination of the laminar model reflected instability in the real flow, i.e. a transition from laminar to turbulent flow.

3.3.4. *Justification for the introduction of artificial initial condition*

The introduction of a slip wall condition was intended to trigger an initial disturbance in the flow field. This procedure is justified since our interest is restricted

to the solutions after the effect of the initial disturbance has decayed: for flows at $Re = 32.5 > Re_c$, identical self-sustained flow oscillations were produced through (i) a brief imposition of a slip condition on a portion of one of two disk walls when the entire radial channel was initially at the (symmetrical) Poiseuille-flow situation, and (ii) using the (asymmetrical) flow field at $Re = 30$ as the initial condition for the computing operation. No disturbance is needed once the periodic flow oscillation becomes self-sustained. Experimentally, the periodic flow-separation phenomenon was also observed in the air-flow apparatus of figure 7 with a single-stream influx as well as in the liquid-flow setup of figure 1 having a double-stream influx. This indicates that the phenomenon is unaffected by the initial disturbance.

4. Comparison between experiments and theory

Comparison between the theory and flow-visualization experiments is made based on a pair of parallel disks with s/d_1 of 0.075 (0.078 for the experiments, to be precise). (*a*) The critical Reynolds number Re_c for vortex formation to occur was predicted by the theory to be between 27.5 and 30.0, while the experiments provided a value of Re_c of about 29, as shown in figure 4. (*b*) This apparatus produced an almost uniform approach flow at the plate entrance, which was employed as the inlet condition in the theoretical analysis. (*c*) The points of inflexion in the velocity profiles near the entrance were predicted by the theory and experimentally confirmed. (*d*) Both theory and experiments indicate that the separation point (implying the nucleation site) moves upstream with increasing Re. More shifting was observed in the experiments than predicted. (*e*) The theory indicated the divergence of the flow field at Re_t between 34.0 and 35.0. In the experiment, a transition from laminar to turbulent flow occurred at $Re = 45.5$ but was not observed at $Re = 31.4$. Therefore, Re_t must lie between 31.4 and 45.5, which confirms the theory.

5. Conclusions

A flow-visualization study has disclosed that, as Re is increased from 1.5 to 50.0, the steady-influx radial flow between parallel disks follows three distinct patterns: (i) steady flow without separation and reattachment of the shear layer with $Re < Re_c$; (ii) a self-sustained flow oscillation which decays downstream in the range of $Re_c \leqslant Re < Re_t$; and (iii) a self-controlled flow fluctuation followed by a laminar-to-turbulent transition and subsequent reverse transition along the flow passage, when $Re > Re_t$. The flow unsteadinesses in (ii) and (iii) are caused by a vortex street composed of vortices that separate periodically and alternately from both plates. Finite-difference numerical solutions of the unsteady vorticity-transport equation are in partial agreement with the experimental observations. Hot-wire measurements have confirmed that periodic variations in the radial velocities are axisymmetrical in nature. The study demonstrates that the phenomena of shear-layer separation and reattachment in the radial flow between parallel disks are, contrary to common supposition, unsteady. Once initiated, the sequence of nucleation, growth, migration and decay of these vortices is self-sustained. The mechanism needs to be explored further.

The authors wish to express their gratitude to Messrs K. Numata, A. Fujii, H. Ohba and A. Nishino for their assistance in carrying out the experiment and

numerical calculations. The study was partially supported by the Ministry of Education of the Japanese Government (Grant C. 1981) and by National Science Foundation of the U.S. Government under Grant Number ME 80-18031.

REFERENCES

BAKKE, E., KREIDER, J. F. & KREITH, F. 1973 Turbulent source flow between parallel stationary and co-rotating discs. *J. Fluid Mech.* **58**, 209.

BENENSON, D. & BOTT, J. F. 1961 Two-dImensional laminar boundary-layer flow within a diffuser. *Am. Soc. Mech. Engrs, paper No.* 61-WA-193.

DAVIS, W. & FOX, R. W. 1967 An evaluation of the hydrogen bubble technique for the quantitative determination of fluid velocities within clear tubes. *Trans. ASME* D: *J. Basic Engng* **89**, 778.

HUNT, J. B. & TORBE, I. 1962 Characteristics of hydrostatic thrust bearings. *Intl J. Mech. Sci.* **4**, 503.

ISHIZAWA, S. 1965 The axi-symmetric laminar flow in an arbitrary shaped narrow gap, 1st Report. *Bull. Jap. Soc. Mech. Engrs* **8**, 353.

ISHIZAWA, S. 1966 The axi-symmetric laminar flow in an arbitrary shaped narrow gap, 2nd Report. *Bull. Jap. Soc. Mech. Engrs* **9**, 86.

JACKSON, J. D. & SYMMONS, G. R. 1965*a* The pressure distribution in a hydrostatic bearing. *Intl J. Mech. Sci.* **7**, 239.

JACKSON, J. D. & SYMMONS, G. R. 1965*b* An investigation of laminar radial flow between two parallel discs. *Appl. Sci. Res.* **A15**, 59.

JENSEN, V. G. 1959 Viscous flow round a sphere at low Reynolds numbers (40). *Proc. R. Soc. Lond.* A **249**, 346.

LICHT, L. & FULLER, D. D. 1954 A preliminary investigation of an air lubricated hydrostatic thrust bearing. *Am. Soc. Mech. Engrs paper No.* 54-LUB-18.

LIVESEY, J. L. 1960 Inertia effects in viscous flows. *Intl J. Mech. Sci.* **1**, 84.

MOLLER, P. S. 1963 Radial flow without swirl between parallel discs. *Aero. Quart.* **14**, 163.

MORGAN, D. G. & SAUNDERS, A. 1960 An experimental investigation of inertia effects in viscous flow. *Intl J. Mech. Sci.* **2**, 8.

NARASIMHA, R. & SREENIVASAN, K. R. 1979 Relaminarization of fluid flows. *Adv. Appl. Mech.* **19**, 221.

RAAL, J. D. 1978 Radial source flow between parallel discs. *J. Fluid Mech.* **85**, 401.

SAVAGE, S. B. 1964 Laminar radial flow between parallel plates. *Trans. ASME* E: *J. Appl. Mech.* **31**, 594.

SCHRAUB, F. A., KLINE, S. J., HENRY, J., RUNSTADLER, P. W., JR., & LITTELL, A. 1965 Use of hydrogen bubbles for quantitative determination of time-dependent velocity fields in low-speed water flows. *Trans. ASME* D: *J. Basic Engng* **87**, 429.

STERNBERG, J. 1954 The transition from a turbulent to a laminar boundary layer. *BRL Report* 906, *Ballistic Research Laboratories, Aberdeen Proving Ground, Maryland.*

WILSON, S. D. R. 1972 A note on laminar radial flow between parallel plates. *Appl. Sci. Res.* **25**, 349.

WOOLARD, H. W. 1954 A study of the flow in a narrowly-spaced radial diffuser. ME thesis, University of Buffalo, NY.